

Mission Opportunities for the Flight Validation of the Kinetic Impactor Concept for Asteroid Deflection

Sonia Hernandez^{a,1,*}, Brent W. Barbee^{b,2}, Shyam Bhaskaran^{c,3}, Kenneth Getzandanner^{b,2}

^aThe University of Texas at Austin, 210 E. 24th St., Austin, TX, 78712, USA, 512.471.7593

^bNASA/GSFC, Code 595, 8800 Greenbelt Road, Greenbelt, MD, 20771, USA

^cJet Propulsion Laboratory/California Institute of Technology, 4800 Oak Grove Dr., Pasadena, CA, 91109

Abstract

The kinetic impactor technique for deflecting near-Earth objects (NEOs), whereby a spacecraft is directed to collide with a NEO to alter its orbit via momentum transfer, is one of several proposed methods for defending Earth against hazardous NEOs (asteroids and comets). In this paper we present detailed mission design concepts for a notionally feasible and affordable kinetic impactor flight validation mission deployed to a currently known near-Earth asteroid (NEA). Several filter steps are devised that utilize relevant criteria to optimally balance key parameters, such as approach phase angle, estimated NEA diameter, relative velocity at intercept, and current NEA orbit knowledge, and produce refined lists of the most promising candidate target NEAs.

Keywords: kinetic impact, asteroid deflection, mission design, trajectory optimization, flight validation

1. Introduction

The kinetic impactor technique for deflecting near-Earth objects (NEOs), whereby a spacecraft is directed to collide with a NEO to alter its orbit via momentum transfer, is one of several proposed methods for defending Earth against hazardous asteroids and comets. NEOs are asteroids and comets whose orbit perihelia are < 1.3 AU, which means that they approach or cross Earth's orbit, creating the possibility of collisions with Earth. NEOs consist of both near-Earth asteroids (NEAs) and near-Earth comets (NECs).

The kinetic impactor technique must be validated by one or more flight validation missions in order to be considered reliable during an actual incoming NEO scenario, but such flight validation missions have yet to be performed. In previous work [1] a survey was performed on a subset of the known NEA population whose orbits are completely exterior or interior to Earth's orbit (for safety reasons) to identify all target NEAs that offer notionally feasible opportunities for kinetic impactor flight validation missions. The previous survey was conducted using a filter that is based on optimized mission mass. Also, a detailed model was developed for predicting the deflection of the NEA's orbit as a proxy for the experimental observability of the change in the NEA's velocity.

The subpopulation of NEAs chosen for our study are those whose orbits are entirely exterior or interior to Earth's orbit. By choosing NEAs for the proposed test missions whose orbits do not cross Earth's orbit, we ensure that Earth will not be threatened by the flight validation missions, regardless of what might go wrong during the experiments. We also seek low ΔV missions for the sake of affordability, and therefore only selected NEAs with heliocentric orbit inclination $\leq 20^\circ$ for this study. Besides safety and affordability, an additional constraint is that the deflection imparted to the NEA by the kinetic impactor must be easily measured by an observer spacecraft that has rendezvoused with the NEA prior to the collision of the kinetic impactor. The mission trajectories are designed such that the observer and impactor launch together on a single launch vehicle into an Earth escape

*Corresponding author

Email addresses: sonia.hernandez@utexas.edu (Sonia Hernandez), brent.w.barbee@nasa.gov (Brent W. Barbee), shyamkumar.bhaskaran@jpl.nasa.gov (Shyam Bhaskaran), kenneth.getzandanner@nasa.gov (Kenneth Getzandanner)

¹Graduate Student, Department of Aerospace Engineering and Engineering Mechanics

²Aerospace Engineer, Navigation and Mission Design Branch

³Supervisor for the Outer Planet Navigation Group

trajectory that takes the observer directly to rendezvous with the NEA. The impactor separates from the observer after launch but before observer arrival at the NEA by performing a maneuver such that it will collide with the NEA after the observer has spent adequate time gathering data on the NEA. This trajectory design is chosen over other types of missions, such as launching the observer and impactor spacecraft on two separate launch vehicles, in order to reduce the cost of the mission. To ensure a measurable experiment we require that the difference in position between the NEA's deflected and undeflected orbits reach at least 100 km by 2 years after impact.

We build upon the results from the previous study [1] by augmenting the target NEA filter to incorporate additional criteria such as the approach phase angle of the spacecraft with respect to the NEA. The approach phase angle should be $\leq 90^\circ$ to provide an operationally realistic scenario in which the spacecraft's onboard sensors are able to acquire the NEA (by virtue of the NEA being adequately illuminated from the spacecraft's perspective) during approach and terminal guidance. Additionally, new filter steps are devised that utilize all criteria to optimally balance key parameters such as approach phase angle, estimated NEA diameter, relative velocity at intercept, and current NEA orbit knowledge to produce a refined list of the most promising candidate target NEAs for future flight validation missions.

Finally, we combine all of the aforementioned analysis to produce complete detailed mission designs for notionally feasible and affordable kinetic impactor flight validation test missions deployed to currently known target NEAs. We provide extensive detail on the trajectory design, terminal guidance, and orbit determination for a specific mission to NEA 1998 KG₃. We also present a list of the most promising target NEAs for kinetic impactor flight validation test missions.

2. Notional Flight Validation Mission Target Selection

Here we describe our methodology for surveying the NEA population to identify the best candidates for kinetic impactor flight validation missions, beginning with an overview of the known NEA population and its subgroups.

2.1. Initial NEA Candidate Population

We begin with a brief overview of the NEAs used in this study, which are based on the NEA population used in Ref. 1. NEAs are classified into four groups based on their orbital characteristics:⁴

1. *Amors* have orbits exterior to Earth's. The perihelion of an Amor's orbit is therefore between 1.017 and 1.3 AU. There were 3017 Amors known at the time of our study (late June of 2011).
2. *Apollos* are Earth-crossing NEAs with semi-major axes larger than Earth's (> 1 AU), but with perihelia less than 1.017 AU. There were 4392 Apollos known at the time of our study and they continue to comprise the majority of the currently known NEA population.
3. *Atens* are Earth-crossing NEAs, with semi-major axes smaller than Earth's (< 1 AU), but with aphelia greater than 0.983 AU. There were 660 Atens known at the time of our study.
4. *Atiras* have orbits completely interior to Earth's and therefore have aphelia less than 0.983 AU. There were only 11 known Atiras at the time of our study and only 1 more has been discovered since. It is possible that many more exist but are difficult to find using ground-based observatories since Atiras spend most of their orbits in our daytime sky.

Apollos and Atens tend to be more accessible, in terms of low ΔV , to spacecraft missions because they are Earth-crossing NEAs and their orbits are often rather similar to Earth's orbit. However, for our study we selected only Amor and Atira NEAs as candidate mission targets because their orbits are either completely exterior or interior to Earth's orbit. This ensures that Earth will never be threatened by deflection system testing activities, regardless of what might go wrong during the the test missions. Additionally, we imposed the constraint of heliocentric orbit inclination $\leq 20^\circ$ in the interests of keeping mission ΔV manageable. Thus, the candidate target NEAs for our study consist of the 2185 Amor and Atira NEAs with inclination $\leq 20^\circ$; of these, only 5 are Atiras. Figure 1 shows the relationship between heliocentric orbit eccentricity and semi-major axis for all of these NEAs.⁵

To further constrain the set of candidate NEAs, we considered only NEAs with estimated diameters ≥ 95 m as it may be difficult for the terminal guidance systems onboard the observer and impactor spacecraft to successfully locate, identify, and track NEAs with smaller diameters. A NEA's estimated diameter, in units of km, is computed

⁴<http://neo.jpl.nasa.gov/neo/groups.html>. Accessed on 2012-01-23.

⁵The list of NEAs was obtained from the JPL Small-Body Database (SBDB) Search Engine, http://ssd.jpl.nasa.gov/sbdb_query.cgi, on 06/30/2011, and the corresponding ephemeris files were then obtained from the JPL Horizons system, <http://ssd.jpl.nasa.gov/?horizons>.

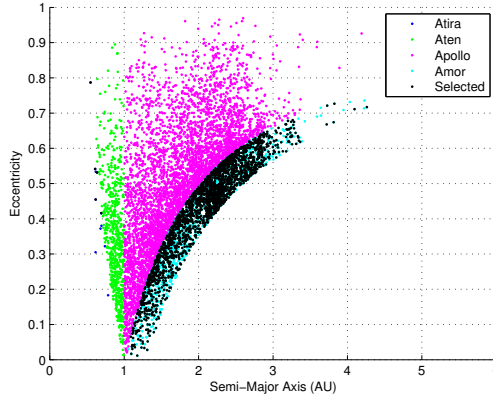


Figure 1: Semi-major axis versus eccentricity for the NEA population.

using its absolute magnitude (a measure of optical brightness), H , and an assumed geometric albedo (indicative of surface reflectivity), p , according to [2]

$$D = \frac{1329}{\sqrt{p}} 10^{-0.2H} \quad (1)$$

For most NEAs, p will generally range between 0.05 and 0.25, so we use the average value of 0.15 for our study. The value of H for each NEA is obtained from the Jet Propulsion Laboratory (JPL) Small-Body Database (SBDB) Search Engine. Of the 2185 NEAs first identified in our analysis, 1556 have $D \geq 95$ m.

The set of candidate NEAs considered in our study is constrained even further by defining a criterion for the maximum total ΔV that the observer spacecraft may perform to rendezvous with the NEA, which is explained in Section 2.2.1. This constraint is similar to that defined in Ref. [1].

2.2. Single Launch Trajectory Design

A major requirement imposed on our solution is that the observer spacecraft must arrive between 3 months and 3 years prior to the impactor's collision with the NEA in order to provide the observer spacecraft adequate time to gather data on the NEA prior to the impact. Since the observer is able to study the NEA both before and after the impact, it will be able to collect a wealth of data on the NEA's pre- and post-impact state, thus providing accurate characterization of the effects of the kinetic impact. There are several launch options that we initially considered for sending the observer and impactor spacecraft to the NEA within constraints.

A scenario in which the two spacecraft are launched on separate launch vehicles was considered in Ref. 1, but is not used for this study because of the additional cost associated with two separate launches. In order to achieve an affordable mission design, we instead consider a one-launch case, in which the observer and impactor spacecraft are co-manifested on a single Atlas V 551 launch vehicle that directly injects the observer/impactor spacecraft stack into a hyperbolic Earth departure trajectory. Some time after launch, the impactor separates from the observer and performs a maneuver that leads to a later impact while the observer spacecraft continues traveling to the NEA and arrives prior to the impactor.

The trajectory design is performed in two main steps: First, the observer trajectory is designed based on a conic Lambert solution. Next, the impactor trajectory is designed using the observer spacecraft trajectory as a set of possible initial conditions for the impactor spacecraft.

2.2.1. Observer Trajectory and Constraints

We begin the trajectory design by creating an algorithm that uses a trajectory grid scan technique to assess the suitability of each candidate NEA by computing all possible trajectories to the NEA for observer spacecraft rendezvous. As described previously, we begin by only computing the observer rendezvous solutions because the impactor trajectory will depart from some point on the observer trajectory. Additionally, we can eliminate NEAs from further consideration if they do not offer sufficiently low ΔV rendezvous opportunities for the observer. The methodology we developed for our analysis was inspired by the Near-Earth Object (NEO) Human Space Flight (HSF) Accessible Targets Study (NHATS)⁶, which utilizes broad trajectory survey techniques to identify all NEAs that offer round-trip trajectory opportunities within a specific performance envelope [3]. A schematic of the parameter space structure of this algorithm is provided in Figure 2. Two-body dynamics, with the Sun as the

⁶See <http://neo.jpl.nasa.gov/nhats/>, accessed on 2013-03-26.

central body, and the method of patched conics are assumed for the spacecraft, since a Lambert solver is used for the trajectory design, while high-fidelity ephemerides are used for the Earth and NEAs.

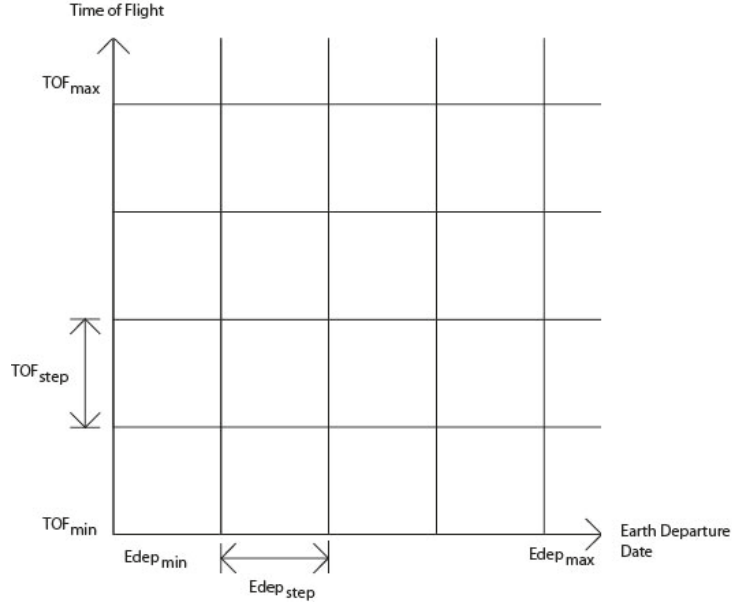


Figure 2: Trajectory grid schematic of the observer

The algorithm varies two independent parameters, departure date and Time of Flight (TOF), within set bounds and uses a Lambert solver to compute the associated rendezvous trajectory ΔV requirements for each combination of departure date and TOF. The constraints applied within the algorithm are summarized in Table 1. For the purposes of mission mass calculations, we assume that our mission uses the Atlas V 551 launch vehicle; using a single existing launch vehicle should help make the proposed missions affordable, even though the Atlas V 551 is the largest (and most expensive) launch vehicle in the Atlas V family.

Table 1: Trajectory constraints for the observer spacecraft

	Observer
Dep. Date Year	2018 - 2022
TOF (days)	≤ 1000
m_{dry} (kg)	≥ 500

The aforementioned 1556 NEAs with $D \geq 95$ m and inclination $\leq 20^\circ$ from the Amor and Atira groups were first subjected to rendezvous trajectory processing using the trajectory grid scanning methods. An Atlas V 551 launch vehicle was assumed for the purposes of computing initial total spacecraft wet mass as a function of Earth departure C_3 . The launch payload mass performance as a function of C_3 for the Atlas V 551 launch vehicle is shown in Figure 3.⁷

Of the 1556 NEAs analyzed in this way, 450 NEAs offer at least one feasible rendezvous trajectory solution set for the observer spacecraft. This initial data set is taken from the results in Ref. 1 (which imposed an additional $\Delta v_{tot} \leq 7$ km/s constraint). Although the asymptotic declination angle associated with Earth departure is not considered, note that the launch vehicle performance data in Figure 3 assume a declination of $\pm 28.5^\circ$, which is commensurate with a launch from the NASA Kennedy Space Center (KSC). In future work we plan to check the Earth departure declinations and only accept trajectory solutions for which the declinations are within the specified range of $\pm 28.5^\circ$.

These trajectory solutions also satisfy the observer spacecraft constraint in Table 1 stating that the final mass of the observer upon NEA arrival must be ≥ 500 kg, based on the aforementioned mass performance of the Atlas V 551 and an assumed observer spacecraft thruster specific impulse of 300 seconds. This final mass constraint was selected to ensure that the observer spacecraft would be sufficiently capable. Note that it is evident that cases that barely meet this ≥ 500 kg arrival mass requirement will not pass the subsequent stages of our analysis because we need excess mass capability to accommodate the impactor and its propellant. The 450 NEAs identified at this stage of the analysis were used as the initial population for subsequent analyses that incorporate the impactor spacecraft.

⁷This data was obtained from <http://elvperf.ksc.nasa.gov/elvMap/>, accessed on 2013-03-13.

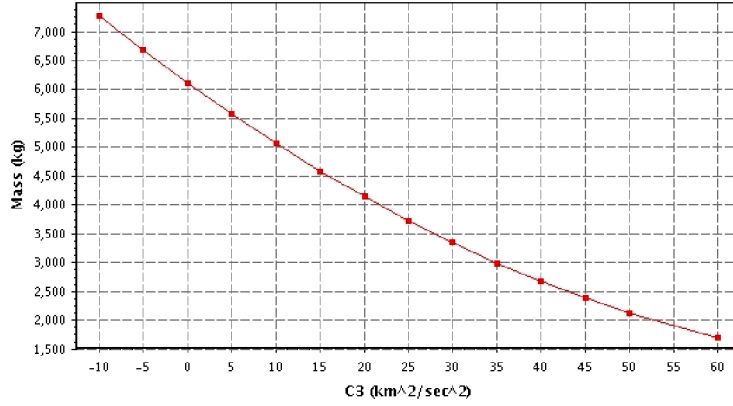


Figure 3: Payload mass performance for the Atlas V 551 launch vehicle.

2.2.2. Impactor Trajectory and Constraints

For each NEA we generate a set of feasible Earth to NEA rendezvous trajectories for the observer spacecraft, as described in Section 2.2.1. Each of these rendezvous trajectories are propagated and used as nominal initial trajectories for the combined observer & impactor trajectory solution. A grid search algorithm is developed to search for all the possible impactor solutions that stem from each viable observer trajectory. A nominal observer solution—the black trajectory depicted in Figure 4—departs Earth at some date $t_{dep,obs}$ and performs a rendezvous with the NEA after a time of flight TOF_{obs} has elapsed. The impactor-search algorithm is written such that the impactor performs a maneuver $\Delta v_{sep,imp}$ after some time t_{sep} has elapsed after Earth departure, such that the impactor spacecraft separates from the observer on a separate trajectory that leads to intercept of the NEA some time after observer arrival at the NEA; this trajectory is shown in red in Figure 4. The maneuver required for the impactor to depart the observer’s NEA rendezvous trajectory is determined by a Lambert solver and the time of flight of the impactor, TOF_{imp} , is constrained to be ≤ 1000 days. Also, recall that we further constrain the flight times such that the observer spacecraft must arrive between 3 months and 3 years prior to the impactor’s collision with the NEA. This ensures that the observer has adequate time to characterize the NEA prior to the kinetic impact.

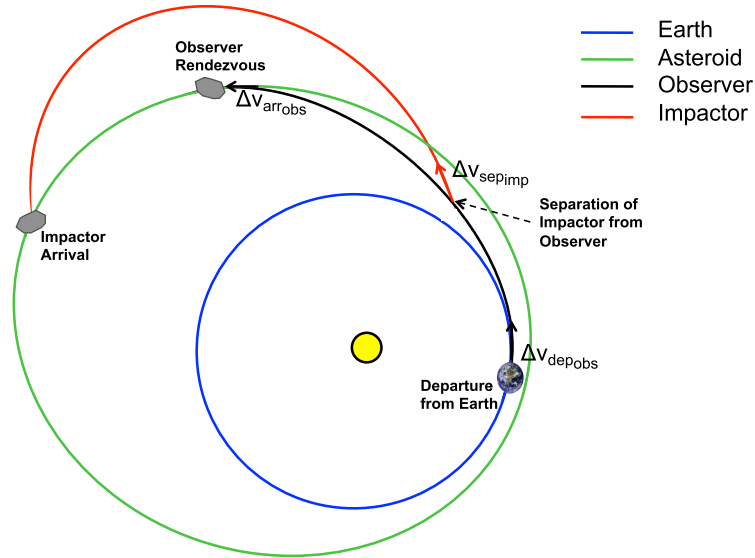


Figure 4: Direct one-launch scenario schematic.

One of the constraints imposed on the algorithm is that the impactor mass at intercept, $m_{imp,dry}$, must be > 0 . This constraint is necessary because the total initial spacecraft mass (observer + impactor) is limited by the launch vehicle performance. The observer dry⁸ mass, $m_{obs,dry}$, is set to 500 kg, a thruster specific impulse, I_{sp} , of 300

⁸By observer “dry” mass we mean the observer mass after the observer performs its major maneuver to rendezvous with the NEA (i.e., match the NEA’s velocity upon arrival at the NEA). This “dry” mass is assumed to include all the necessary propellant for NEA proximity operations after rendezvous.

seconds, corresponding to nominal hypergolic bipropellant propulsion system performance, is assumed for both the observer and the impactor, and the total launch mass, m_{C_3} , is determined as a function of the Earth departure C_3 from the Atlas V 551 launch vehicle performance data shown in Figure 3. The dry mass of the impactor, m_{impdry} , is computed using the ideal rocket equation,

$$\frac{m_{impwet}}{m_{impdry}} = e^{\frac{\Delta v_{imp}}{g_{ISP}}} \quad (2)$$

where $m_{impwet} = m_{C_3} - m_{obswet}$, $m_{obswet} = m_{obsdry} e^{\frac{\Delta v_{arr,obs}}{g_{ISP}}}$, and $\Delta v_{arr,obs}$ is the rendezvous Δv for the observer.

An additional parameter we take into account is the impactor spacecraft approach phase angle with respect to the asteroid. This is important because an operationally realistic NEA intercept mission will require a sufficiently small approach phase angle to facilitate optical acquisition of the NEA by the spacecraft's onboard sensors during terminal guidance. Figure 5 presents a schematic of a spacecraft (blue) approaching an asteroid (gray). The asteroid has an inertial position \mathbf{r}_{nea} and velocity \mathbf{v}_{nea} at the instant before the impact, while the spacecraft has an inertial velocity \mathbf{v}_{sc} . The relative velocity of the spacecraft with respect to the asteroid's velocity is denoted $\mathbf{v}_{sc/nea} = \mathbf{v}_{sc} - \mathbf{v}_{nea}$. The relative approach angle is computed as

$$\begin{aligned} \phi &= \cos^{-1} [(-\hat{\mathbf{v}}_{sc/nea}) \cdot (-\hat{\mathbf{r}}_{nea})] \\ &= \cos^{-1} (\hat{\mathbf{v}}_{sc/nea} \cdot \hat{\mathbf{r}}_{nea}) \end{aligned} \quad (3)$$

and we only consider cases with $\phi \leq 90^\circ$ for the study presented herein.

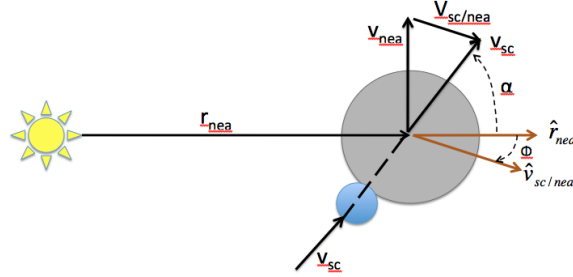


Figure 5: Impactor spacecraft approach angle to the NEA

2.3. Determining Deflection After Impact

When the kinetic impactor spacecraft collides with a NEA, it imparts an impulsive velocity change to the NEA, which leads to a certain amount of deflection of the NEA's heliocentric orbit after some time has elapsed. A detailed model to compute both the impulsive velocity change and the deflection of the NEA's orbit is derived in Ref. 1 and a summary of those results is provided here.

2.3.1. Computing the Change in Velocity Imparted to the NEA

The principle of conservation of linear momentum holds during the impact and a purely plastic collision is assumed, which means that the spacecraft does not bounce off the NEA after the collision. The impulsive velocity change imparted to the NEA, $\Delta \mathbf{v}$, is calculated in the NEA's Radial, In-Track, Cross-Track (RIC) frame at the time of collision [1]. The inertial velocity of the NEA after the impact is given by

$$\mathbf{v}_{nea}^+ = \mathbf{v}_{nea}^- + \Delta \mathbf{v} \quad (4)$$

where \mathbf{v}_{nea}^- is the velocity of the NEA the instant before the collision. The change in velocity in the inertial frame is computed by performing two matrix rotations: the first one from the spacecraft's body frame, B , to the asteroid's RIC frame, and the second one from the RIC frame to the inertial frame, I , according to

$$\Delta \mathbf{v} = (T_I^{RIC})^T (T_{RIC}^B)^T \Delta \mathbf{v}_B \quad (5)$$

The change in velocity in the body frame, B , is given by

$$\Delta \mathbf{v}_B = \begin{pmatrix} \beta \frac{m}{m+M} (v_{sc_{b_1}}^- - v_{nea_{b_1}}^-) & 0 & 0 \end{pmatrix}^T \quad (6)$$

where $v_{sc_{b_1}}^-$ and $v_{nea_{b_1}}^-$ are the first components of the spacecraft and NEA velocities in the B frame [1], m is the mass of the spacecraft, M is the mass of the NEA, and β is the *impact efficiency factor*. One impetus for the

deflection system tests we propose in this paper is that β is currently poorly characterized. Current consensus on the range for β is $1 \leq \beta \leq 5$ [4, 5]. $\beta = 1$ corresponds to a perfectly plastic collision in which the impacting spacecraft is absorbed and no ejecta is produced from the impact crater. $\beta = 2$ corresponds to a perfectly elastic collision in which the momentum of the ejecta is equal and opposite to the momentum of the impactor, and $\beta > 2$ corresponds to a super-elastic collision. For all the results presented herein we assume $\beta = 1$. However, our results are easily expanded to utilize other values of β .

In order to compute the amount by which a NEA is deflected due to an impact, the NEA's mass must be known. However, the mass of a NEA must generally be measured by a spacecraft and so masses are not known for the vast majority of the NEA population. We therefore use the following method to estimate the masses of the NEAs for this study. We assume a spherical shape for each NEA, which allows the NEA's mass, M , to be computed as

$$M = \rho \frac{4}{3} \pi \left(\frac{D}{2}\right)^3 \quad (7)$$

where D is the estimated diameter of the NEA, computed from Eq. (1), and ρ is its assumed density. The density of a NEA will generally range between 1.3 and 8 g/cm³, although the likely value for the density of many NEAs is about 2.6 g/cm³, so we assume this density for the NEAs in our study.

2.3.2. Computing Deflection Due to Impact

Besides safety and affordability, an additional constraint is that the deflection imparted to the NEA by the kinetic impactor must be easily measured by the observer spacecraft. Since a NEA's orbit can generally be determined to within several km or less when a transponder-equipped spacecraft is near the NEA, we require that the deflection of the NEA's orbit be at least 100 km by 2 years after the time of impact to ensure a notionally measurable deflection experiment.

In Ref. [1], two models are presented that can be used to compute the amount by which a NEA's orbit is deflected after a certain amount of time has elapsed. One is an accurate model based on Kepler's equation and the other is an approximate model based on Gauss' form of the Lagrange Planetary Equations. The latter method was proposed by Koenig [6] to compute the deflection when the impact occurs along the NEA's velocity direction at perihelion. That work is expanded in [1] by developing a computationally efficient deflection equation that is valid at any point along the NEA's orbit with any spacecraft impact direction, and this is the model used for the results in this paper.

The approximate deflection of the NEA's orbit at an arbitrary time Δt after the impact is given by

$$\Delta r = 1.5 C \frac{\Delta a}{a} \frac{\Delta t}{T} \quad (8)$$

where T is the period of the NEA's unperturbed orbit, a is its semi-major axis, and C is the approximate circumference of an ellipse, given by Ramanujan as [6]

$$C \approx \pi(a + b) \left(1 + \frac{3x^2}{10 + \sqrt{4 - 3x^2}}\right) \quad (9)$$

where $x = (a - b)/(a + b)$ and b is the semi-minor axis of the NEA's orbit. The change in semi-major axis Δa is given by

$$\Delta a = \frac{2}{\sqrt{1 - e^2}} \sqrt{\frac{a^3}{\mu_s}} [e \sin \nu \Delta v_{\hat{r}} + (1 + e \cos \nu) \Delta v_{\hat{t}}] \quad (10)$$

which stems from the time-derivative of a given by Lagrange's Planetary Equations [7]. In this equation a is the NEA's undeflected heliocentric semi-major axis, μ_s is the Sun's gravitational parameter, e is the NEA's orbital eccentricity, ν is the NEA's true anomaly at the time of impact, and $\Delta v_{\hat{r}}$ and $\Delta v_{\hat{t}}$ are the two components of the change in velocity imparted to the NEA (Eq. (5)) expressed in the RIC frame. Note that the time-derivative of a from Lagrange's Planetary Equations only depends on perturbations from the Radial and In-Track directions; therefore the Cross-Track term does not cause any change in the semi-major axis a .

2.4. Candidate NEAs

A summary of all the constraints placed on the impactor spacecraft is shown in Table 2 and the observer spacecraft constraints are summarized in Table 1.

The proposed algorithm was executed with all the aforementioned observer-impactor spacecraft constraints, along with an added constraint that the Orbit Condition Code (OCC) must be ≤ 2 for each NEA. The OCC is an integer scale for how well a NEA's orbit is known, with 0 representing the best orbit knowledge and 9 indicating

Table 2: Constraints for the Impactor spacecraft.

	Impactor
Arr. Date	$t_{arr_{imp}} - 3 \text{ yr.} \leq t_{arr_{obs}}$
Separation Date from Observer	$t_{arr_{obs}} \leq t_{arr_{imp}} - 3 \text{ mon.}$
	$t_{sep} \geq 1 \text{ mon. from departure date}$
TOF (days)	$t_{sep} \leq 1 \text{ mon. before observer arrival}$
Approach Angle ($^\circ$)	≤ 1000
Deflection (km) after 2 years	≤ 90
	≥ 100

the poorest orbit knowledge. Applying our algorithms to the $OCC \leq 2$ NEAs yielded 3 candidate NEAs that meet all constraints and offer feasible trajectory solutions. These NEAs are shown in Table 3 along with summaries of their minimum approach angle trajectory solutions. Note that while only one observer/impactor mission solution is shown for each NEA, there are in fact thousands of feasible mission solutions for each NEA. The values shown in Table 3 are defined as follows. D is the approximate diameter of the NEA, Type refers to either the Observer (Obs) or Impactor (Imp) trajectory, $\Delta V_{arr_{obs}}$ is the ΔV required for the observer to rendezvous with the NEA, $\Delta V_{arr_{imp}}$ is the relative velocity at impact with respect to the NEA velocity (i.e., v_∞), Separation Date is date of Impactor separation from Observer spacecraft, TOF is the Time of Flight, where TOF for the impactor is measured from separation date from the Observer until impact with NEA, and TBI is the Time Before Impact, measured from Observer arrival date.

Table 3: Candidate NEAs that meet the Observer and Impactor spacecraft requirements.

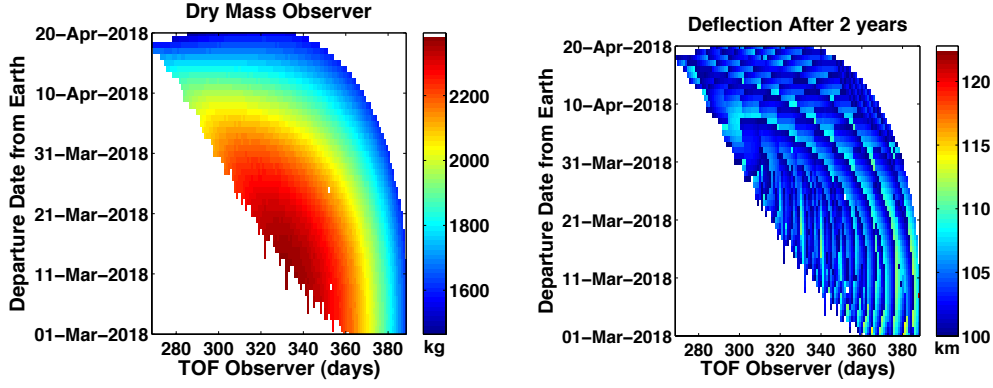
	NEA	D (m)	OCC	Type	Earth Dep. Date	C_3 (km^2/s^2)	ΔV_{arr} (km/s)	Separation Date	ΔV_{sep} (km/s)	TOF (days)	TBI (days)	m_{final} (kg)	Δr (km)	Approach Angle ($^\circ$)
1	1998 KG ₃	123	0	Obs Imp	4-16-2018	16.12	3.04 2.84	10-3-2018	0.9	354 454	270	500 2,280	101.35	11.28
2	2003 SM ₈₄	97	1	Obs Imp	3-27-2021	33.69	1.60 8.11	11-22-2021	8.34	294 874	820	500 132	103.21	30.85
3	2004 EO ₂₀	137	2	Obs Imp	9-22-2019	10.74	3.15 7.68	3-10-2020	6.67	327 997	840	500 367	138.89	36.23

3. Mission Scenario Overview

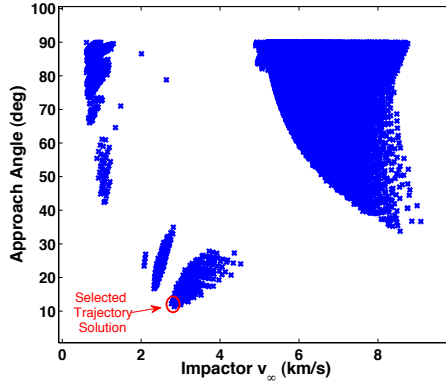
Of the three possible candidate NEAs shown in Table 3, 1998 KG₃ was chosen for further analysis. All three solutions shown for each NEA offer similar results in terms of deflection, since $\Delta r \approx 100$ km after 2 years. However, there are several reasons for choosing 1998 KG₃ over the other two. First, its OCC is 0, which means that its orbit is well known and it will therefore be easier for the spacecraft to locate. Second, both the Observer and Impactor spacecraft TOF are relatively low (≈ 1 year), whereas the Impactor TOF is approximately 3 years for cases 2 and 3 in Table 3. Third, the relative velocity at impact $v_\infty = \Delta V_{arr_{imp}}$ is 2.84 km/s and the approach angle $\phi = 11.28^\circ$, which are much lower than for the other two candidates. That low relative velocity at impact makes this a good initial kinetic impactor test mission by not overstressing the system with a high approach velocity. A case with higher impact velocity would be good for subsequent test missions after the system has been proven with a more mild approach velocity. Fourth, the ΔV required of the impactor for the 1998 KG₃ mission is 0.9 km/s, which is much more operationally realistic than the 8.34 km/s and 6.67 km/s Δv values required of the impactor for the other two cases.

All viable trajectory solutions found for 1998 KG₃ are shown in Figure 6. A contour plot of the Observer spacecraft dry mass $m_{obs,dry}$ is shown in Figure 6(a), where the x -axis is the TOF of the Observer and the y -axis is the Earth departure date. Note that this dry mass corresponds to the initial available mass as computed by the results in Section 2.2.1, i.e., before imposing the constraint in Section 2.2.2 that $m_{obs,dry} = 500$ kg. Figure 6(b), in this case showing the deflection Δr 2 years after impact. The deflections achieved by all the feasible trajectory solutions are tightly bounded, with a difference of only 20 km between the minimum and maximum achieved deflections. Figure 6(c) shows the Impactor spacecraft relative velocity at impact, v_∞ , versus approach angle, ϕ . The trajectory solution with the smallest approach angle was chosen for our notional mission design, and this trajectory solution happens to have a relatively small v_∞ as well.

An ecliptic plane projection of the trajectory solution given in Table 3 for 1998 KG₃ is presented in Figure 7(a), and a three-dimensional view of the trajectory is presented in Figure 7(b). The Observer and Impactor depart



(a) Observer dry mass as a function of Earth departure date and TOF of observer (b) Achieved 2-year Δr as a function of Earth departure date and TOF of observer



(c) Impactor relative arrival velocity v_∞ vs. approach angle relative to NEA

Figure 6: All observer/impactor solution set data for NEA 1998 KG₃.

together from Earth on 4/16/2018, shown in black in Figures 7(a) and 7(b). The Impactor spacecraft separates from the Observer on 10/3/2018 and the Impactor's trajectory is depicted in red. The Observer rendezvous with the NEA on 4/5/2019, and about 9 months later the Impactor spacecraft collides with the NEA. Ecliptic plane projections of the mission trajectories for the other two NEAs in Table 3 are presented in Figure 8 for comparison.

Note that the trajectory design explained in Section 2 and the results shown in this section use a grid search algorithm. For further trajectory analysis, an optimization algorithm is being written in which the initial guess for the trajectory sequence is provided by the grid search algorithm and the objective is to maximize the deflection of the NEA's orbit. The trajectory design shown in Figure 4 remains as is, except that a second maneuver by the impactor, $\Delta \mathbf{v}_{2imp}$, is permitted after a time t_{sep2} has elapsed if it serves to improve overall performance. Accordingly, the performance index, J , can be defined as

$$J = \max \|\Delta \mathbf{r}\|$$

with variables

$$\mathbf{X}_p = \left[t_{dep} \quad \text{tof}_{obs} \quad t_{sep} \quad t_{sep2} \quad \text{tof}_{imp} \quad \Delta \mathbf{v}_{sep_{imp}} \quad \Delta \mathbf{v}_{2imp} \right]_{11 \times 1}^T$$

The equality and inequality constraints are

1. $\mathbf{r}_{obs}(t^*) = \mathbf{r}_{nea}(t^*)$ at time of observer rendezvous $t^* = t_{dep} + \text{TOF}_{obs}$
2. $\mathbf{r}_{imp}(t^*) = \mathbf{r}_{nea}(t^*)$ at time of impact $t^* = t_{dep} + t_{sep} + \text{TOF}_{imp}$
3. Impactor mass $m_{imp_{dry}} > 0$ at intercept

as well as all the constraints outlined in Tables 1 and 2. Development, testing, and implementation of the optimization algorithm is part of ongoing research and we anticipate that it will produce improved results that will be most useful if the candidate mission described herein, or one like it, ever becomes an actual mission.

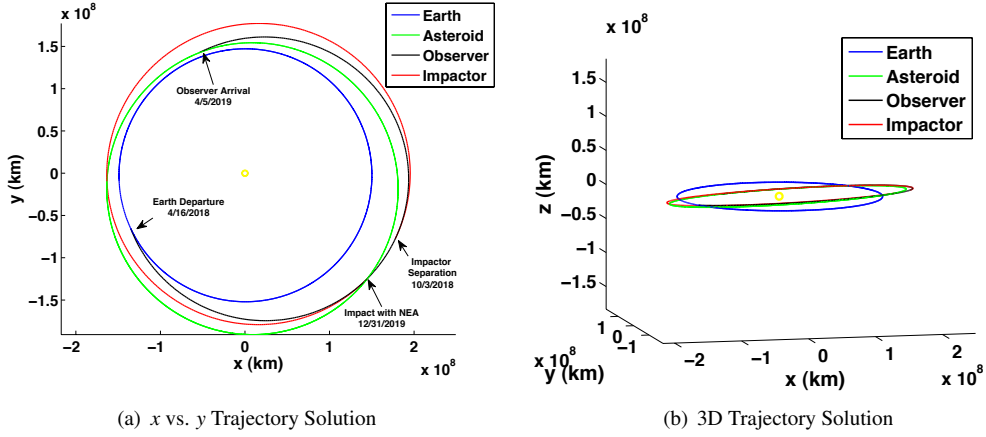


Figure 7: Chosen trajectory solution for NEA 1998 KG₃.

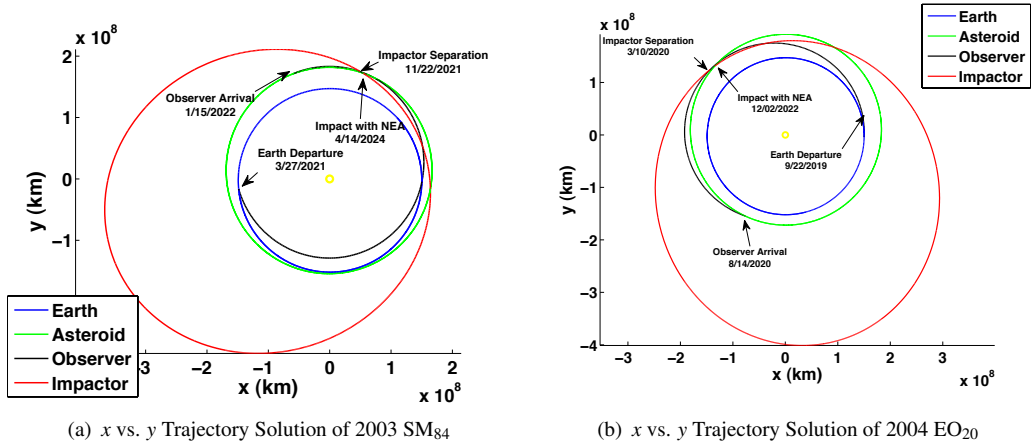


Figure 8: Selected trajectory solutions for NEAs 2003 SM₈₄ and 2004 EO₂₀ as described in Table 3.

3.1. Orbit Determination Analysis

The observer spacecraft will orbit the NEA as it collects optical navigation measurements and physical characterization data. Radiometric tracking will also be performed, including Deep Space Network (DSN) range, Doppler, Delta-Differenced One-Way Range (DDOR) measurements. That will result in a significantly refined ephemeris for the NEA, which will then be used to adjust the kinetic impactor's approach trajectory as needed.

Prior to the arrival of the kinetic impactor, the observer spacecraft will cease orbiting the NEA and move away to a safe distance. The observer will collect imagery and far-field optical navigation data for the NEA from that safe vantage point, including observations of the kinetic impact event itself. After the kinetic impactor collision, the observer spacecraft will re-enter a stable orbit about the NEA and resume nominal operations. As with the pre-impact phase, ground-based radiometric tracking of the observer spacecraft is combined with optical navigation images in the orbit determination process to produce estimates of the post-impact state of the NEA. The NEA state estimates are used to reconstruct the $\Delta\vec{v}$ imparted to the NEA by the kinetic impactor. A detailed covariance analysis of the post-impact scenario for 1998 KG₃ is currently in progress.

Covariance analysis of a similar scenario consisting of a post-impact observer spacecraft in orbit about the NEA 2002 AT₄ is shown in Ref. 8. In that case the data arc spans from two weeks before impact to 30 days after and includes DSN range, Doppler, Delta-Differenced One-Way Range (DDOR), and optical navigation measurements. The results of that analysis suggest that the $\Delta\vec{v}$ reconstruction is sufficiently accurate to measure the post-impact deflection after approximately five days of continuous tracking. Therefore, estimation of the $\Delta\vec{v}$ imparted to 1998 KG₃ should be possible with a similar navigation strategy and we are in the process of executing the necessary simulations to demonstrate that and quantify performance for this particular case.

4. Terminal Guidance Analysis

Terminal guidance navigation to achieve spacecraft impact on the asteroid is accomplished through the use of an onboard autonomous navigation system, called AutoNav. AutoNav has been used successfully on several comet missions (Deep Space 1, Stardust, Stardust NExT, and EPOXI), including the only hyper-velocity impact of a small body to date, Deep Impact (DI). Detailed descriptions of how AutoNav worked for DI can be found in Ref. 9. The extension of AutoNav as applied to the general asteroid impact scenario is described in Ref. 10. Here, we give a brief overview and then show results of a simulation for impacting 1998 KG₃.

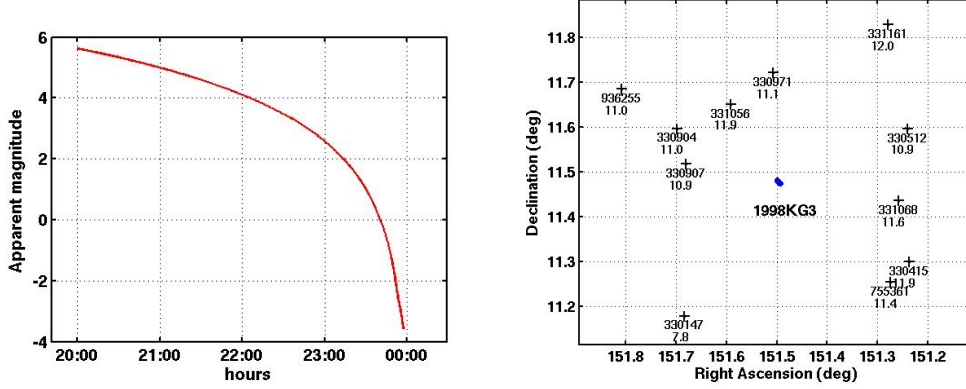
Navigation of the observer spacecraft through all mission phases, and the impactor through all phases except the terminal guidance, can be accomplished using standard ground-based navigation techniques. For the terminal guidance of the impactor, however, the rapid pace of events and the restrictions imposed by the round-trip light time preclude the ground-based approach. Thus, a completely self-contained onboard system such as AutoNav must be used. The purpose of AutoNav is to take navigational data in the form of optical images of the target asteroid, determine the spacecraft's position and velocity relative to the asteroid, and perform and execute maneuvers to guide the spacecraft to the intended location. Thus, AutoNav has three main components: (1) image processing to extract the observable information from the images, (2) orbit determination (OD) to ingest the observable information into a least-squares filter to compute the orbit, and (3) maneuver algorithms to compute discrete $\Delta\vec{v}$ maneuvers at specified times, and turn the $\Delta\vec{v}$ vector into commands to orient the spacecraft and fire the proper thrusters to achieve the desired $\Delta\vec{v}$. Detailed descriptions of the algorithms and procedures for all three components can be found in Ref. 10.

The images used by AutoNav are typically from a space-qualified camera in which the camera lens focuses light onto a Charge-Coupled-Device (CCD) pixel array. The CCD output is the light intensity over the array in digital form, which can then be used by the image processing system. For this study, we chose to use the DI Medium Resolution Imager (MRI) camera which was used on the DI impactor spacecraft. This camera has a focal length of 2100 mm, and a CCD array of 1024 square pixels. The resulting field-of-view (FOV) is 0.6°; the resolution of a single pixel, the IFOV, is 10 μ rad. The purpose of the image processing is to extract the center-of-brightness (COB) from the image of the asteroid. When the asteroid is unresolved (its angular extent is less than one pixel), Gaussian techniques can be used. As the asteroid becomes resolved (angular extent greater than a pixel), a moment algorithm can be used. For the 1998 KG₃ scenario and the MRI camera, the asteroid becomes resolved at 72 minutes prior to impact.

As described in Ref. 10, a major consideration for AutoNav is whether stars are visible in the frame along with the asteroid. If they are, then they can be used to determine the exact inertial pointing of the camera; if not, then the onboard Inertial Measurement Unit (IMU) must be used. The latter introduces error into the OD process which degrades the accuracy of the targeting. For our scenario, we can determine the brightness of the asteroid during the terminal guidance phase (the period of 4 hours to 2 minutes prior to impact), using the optical parameters of the asteroid described in Section 2. The result is shown in Figure 9(a), where it can be seen that the visual magnitude ranges from about 6 at the start to -4 at the end. In Figure 9(b), the visual magnitudes of the background stars are shown, along with the path of 1998 KG₃ against these stars for the terminal guidance phase. As can be seen, the visual magnitudes of the background stars range from 7.8 to 12.0, much dimmer than the asteroid. Thus, we assume in this study that we must rely on the IMU for attitude; we baseline a Scalable Space Inertial Reference Unit (SSIRU) class gyroscope, with associated drift and angle random walk values as shown in Table 4.

The terminal guidance accuracy for the 1998 KG₃ scenario is determined through the use of Monte Carlo simulations. In the simulation setup, a "truth" model for the trajectory and observations is obtained from sampling the error sources given in Table 4. As the truth trajectory is propagated, AutoNav is fed images generated from this trajectory, along with pointing errors associated with the IMU; from this, AutoNav computes OD solutions and computes maneuvers. The maneuvers are implemented on the truth side using the execution errors sampled from the errors given in the table. As the truth trajectory either impacts or flies by 1998 KG₃, the simulation is stopped. This process is repeated for 500 runs to produce the impact statistics.

The terminal guidance phase for each simulation run begins at Impact (I) $-$ 4 hours. This time period was chosen to ensure that the asteroid will be in the camera FOV at the start of AutoNav. With the initial target relative position error shown in Table 4, due primarily to the uncertainty in the heliocentric orbit of 1998 KG₃, later start times might result in never seeing the asteroid in the 0.6° FOV camera. After taking a set of images for 10 minutes at a rate of one every minute, the first OD is performed. The accumulation of data allows for robust data editing to remove any outliers and ensure a stable solution. Subsequently, an OD is performed after every image is taken. As was done for DI, 3 maneuvers are performed at I $-$ 1 hour, I $-$ 30 min, and I $-$ 2 min. The first is to remove the initial ephemeris errors, the second is to clean up any execution error from the first, and the final provides the best possible chance to impact a spot on the surface. For simulating images of 1998 KG₃, we use a triaxial ellipsoid shape model. Given a nominal diameter of 123 m, we use an assumed aspect ratio of 2:1, which results in the



(a) Apparent magnitude of 1998 KG₃ during terminal guidance phase. (b) Apparent magnitude of background stars during terminal guidance phase.

Figure 9: Apparent magnitudes of 1998 KG₃ and background stars.

Table 4: Simulation truth model error sampling.

Parameter	Error Sampling(1σ)
Trajectory	
Position	50 km
Velocity	5 cm/s
Maneuver Execution Error	
Fixed magnitude	4.3 mm/s
Proportional magnitude	10%
Fixed direction	4 mm/s
Proportional direction	3.1%
IMU Bias and Drift	
Rate Bias	0.0005 °/s
Angle Random Walk	0.0005 °/√hr
Asteroid Orientation	
Pole RA	360° (uniform)
Pole DEC	90° (uniform)

major axes of the ellipsoid being $196 \times 98 \times 98$ m. Since the orientation of the target asteroid will not be known for the general impact mission scenario, we sample a uniform distribution for the pole orientation as shown in Table 4, parametrized by pole right ascension (RA) and declination (DEC).

The results of the Monte Carlo runs show 497 out of the 500 samples (99.4%) successfully impacting the asteroid. Figure 10 graphically shows the impact locations, first as inertial impact locations in the inertial target plane centered on the asteroid and perpendicular to the incoming spacecraft asymptote, and second as actual locations on the surface of the ellipsoid representing 1998 KG₃. In the first, the dashed line represents a notional 123 m circle indicating the approximate diameter of 1998 KG₃, where it can be seen that the majority of locations are within 25 m of the center. The slight offset from center is due to the COB not being at the asteroid center as a result of the 11° approach phase angle. Figure 10(b) shows that the impact locations are scattered across most of the asteroid's surface; this is due to the pole orientation being randomly sampled.

5. Conclusions

Near-Earth asteroids (NEAs) of sufficient energy (mass and impact velocity) to cause substantial damage have collided with Earth in the past and will do so again in the future. It is imperative that we begin testing candidate NEA deflection systems, such as the kinetic impactor, on harmless NEAs now, so that we will be prepared before an imminent threat is discovered. In this paper we built upon previous work [1] in which a survey of the known

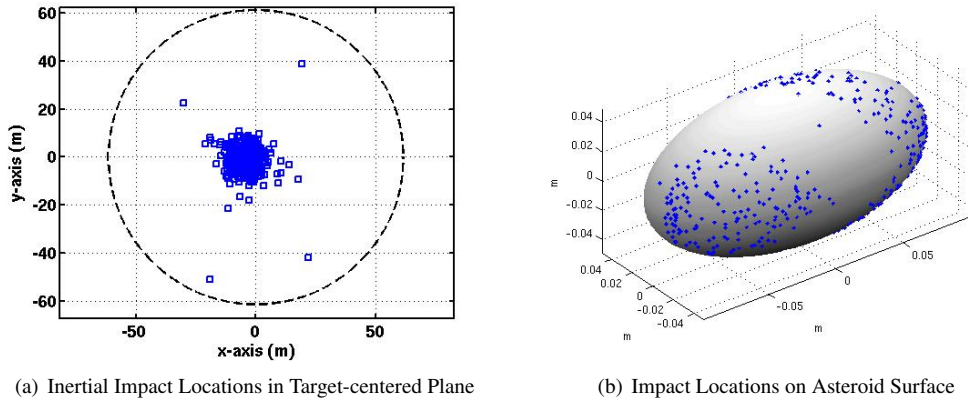


Figure 10: Impact locations from Monte Carlo simulation.

NEA population was performed to identify NEAs that may be good targets for kinetic impactor deflection test missions by virtue of offering safe and affordable mission scenarios that are likely to yield measurable results.

One of the main design concepts we propose is that the deflection imparted to the NEA by the kinetic impactor must be readily measured by an observer spacecraft that has rendezvoused with the NEA prior to the collision of the kinetic impactor. The trajectory is designed such that the observer and impactor launch together on a single launch vehicle directly into an Earth escape trajectory that takes the observer to rendezvous with the NEA. The impactor separates from the observer after launch but before observer arrival at the NEA by performing a maneuver such that it will collide with the NEA after the observer has spent adequate time gathering data on the NEA. Additionally, new filter steps are devised that utilize all criteria to optimally balance key parameters such as approach phase angle, NEA diameter, relative velocity at intercept, and current NEA orbit knowledge to produce a refined list of the most promising candidate target NEAs for a future flight validation mission.

Three candidate NEAs have been found to satisfy all the requirements, each providing multiple trajectory options. A detailed trajectory analysis is performed for NEA 1998 KG₃, as well as a detailed terminal guidance analysis and an orbit determination study. The mission scenarios we have designed for these NEAs all have Earth departure dates during the years 2018 to 2022 and therefore represent near-term opportunities for safe, affordable, and meaningful deflection test missions. These missions have the potential to provide humanity with the tools necessary to avert one of the deadliest natural disasters ever to affect our planet.

5.1. Future Work

We have identified a number ways to improve our algorithms and are pursuing these as future work items. For the spacecraft departure phase, we plan to check the Earth departure asymptote declinations and only accept trajectory solutions for which the declinations are within a specified range commensurate with launch vehicle performance specifications. We currently do not impose a constraint on Δv maneuvers performed by the observer or impactor spacecraft, and to address that we plan to enforce constraints in our code such that no mission solutions are accepted if the magnitude of any maneuver in the mission sequence exceeds a specified value. We will also expand our trajectory design techniques to help ensure that we can find feasible solutions (particularly with constraints on maneuver magnitudes) by implementing a multi-revolution Lambert solver and incorporating deterministic Deep Space Maneuvers (DSMs) when they serve to help minimize propellant mass requirements; we are also considering incorporating planetary flybys for gravity assists. Those changes will lead to longer flight times for both the observer and impactor in some cases, but longer flight times are more operationally realistic and affordable than very large maneuvers that satisfy the ideal rocket equation but require the spacecraft to be mostly propellant.

After implementing and verifying these enhancements to our algorithms we will use them to re-assess mission opportunities to the known Amor and Atira NEAs; over 680 Amor NEAs have been discovered since we defined our population of candidate target NEAs in late June of 2011, and some of them may prove to be attractive targets for our flight validation mission concept. We will also implement the optimization algorithm described herein to formally optimize the mission solution according to a defined performance index (e.g., maximize NEA deflection), allowing for multiple maneuvers, and apply the optimization algorithm to the best of the results from our improved trajectory grid searches. Finally, we will model the most likely impact vector from the terminal guidance analysis to produce a refined prediction for the effect of the impact on the NEA's orbit. This will become

an input for simulation of the pre- and post-impact OD for the NEA to quantify the accuracy with which the actual $\Delta\vec{v}$ imparted to the NEA and β can be estimated.

Acknowledgments

Part of this research was carried out at the Jet Propulsion Laboratory, California Institute of Technology, under a contract with the National Aeronautics and Space Administration.

References

- [1] Hernandez, S. and Barbee, B. W., Design of Spacecraft Missions to Test Kinetic Impact for Asteroid Deflection, in: Advances in the Astronautical Sciences, volume 143, Univelt, Inc., San Diego, CA, 2012, pp. 399–418.
- [2] S. R. Chesley, *et al.*, Quantifying the Risk Posed by Potential Earth Impacts, *Icarus* 159 (2002) 423–432. Doi:10.1006/icar.2002.6910.
- [3] B. W. Barbee, R. G. Mink, D. R. Adamo, C. M. Albeding, Methodology and Results of the Near-Earth Object (NEO) Human Space Flight (HSF) Accessible Targets Study (NHATS), in: Advances in the Astronautical Sciences, volume 142, Univelt, Inc., San Diego, CA, 2011, pp. 613–632.
- [4] B. Kaplinger, B. Wie, J. Basart, A Preliminary Study on Nuclear Standoff Explosions for Deflecting Near-Earth Objects, in: 1st IAA Planetary Defense Conference, Granada, Spain. 2009.
- [5] K. A. Holsapple, The Scaling of Impact Processes in Planetary Science, *Annual Review of Earth and Planetary Sciences* 21 (1993) 333–373.
- [6] J. D. Koenig, C. F. Chyba, Impact Deflection of Potentially Hazardous Asteroids Using Current Launch Vehicles, in: *Science and Global Security*, 15, pp. 57–83. 2007.
- [7] B. D. Tapley, B. E. Schutz, G. H. Born, *Statistical Orbit Determination*, Elsevier Inc., 2004.
- [8] S. Bhaskaran, S. Chesley, R. Park, A. Petropoulos, J. Sims, D. Yeomans, Navigation Challenges of a Kinetic Energy Asteroid Deflection Spacecraft, in: Proc. AIAA/AAS Astrodynamics Specialist Conference, Honolulu, Hawaii.
- [9] D. Kubitschek, N. Mastrodemos, R. Werner, B. Kennedy, S. Synnott, G. Null, S. Bhaskaran, J. Riedel, A. Vaughan, Deep Impact Autonomous Navigation: The Trials of Targeting the Unknown, AAS Guidance and Control Conference (2006). Paper AAS 06-081.
- [10] S. Bhaskaran, B. Kennedy, Closed Loop Terminal Guidance Navigation for a Kinetic Impactor Spacecraft, Proceedings of the 2013 IAA Planetary Defense Conference (2013). Paper number IAA-PDC13-04-02.

Copyright © 2013 International Academy of Astronautics. No copyright is asserted in the United States under Title 17, US Code. The US Government has a royalty-free license to exercise all rights under the copyright claimed herein for Governmental Purposes. All other rights are reserved by the copyright owner.